Journal of Photochemistry and Photobiology 10 (2022) 100114

Contents lists available at ScienceDirect

Journal of Photochemistry and Photobiology

journal homepage: www.sciencedirect.com/journal/journal-of-photochemistry-and-photobiology

Synthesis and *in vitro* evaluation of a novel thienopyrimidine with phototoxicity towards rat glioma F98 cells

Odrun A Gederaas [a,b,*], Andreas S Sørensen [a], Mikael Lindgren [b], Thor Bernt Melø [b], Dag Altin [c,d], Ellen MS Flatby [e], Anders Høgset [f], Bård Helge Hoff [a,**]

[a] Faculty of Natural Sciences, Department of Chemistry, Norwegian University of Science and Technology, Gløshaugen, NO-7491 Trondheim, Norway
[b] Faculty of Natural Sciences, Department of Physics, Norwegian University of Science and Technology, Gløshaugen, NO-7491 Trondheim, Norway
[c] BioTrix, Finn Bergs Veg 3, N-7022 Trondheim, Norway
[d] Faculty of Natural Sciences, Norwegian University of Science and Technology, Gløshaugen, NO-7491 Trondheim, Norway
[e] Norwegian University of Science and Technology, University Library, NO 7491 Trondheim, Norway
[f] PCI Biotech AS, 0379 Oslo, Norway

ARTICLE INFO

Keywords:
Pyrimidine
Cytotoxicity
PDT
Photophysics
In vitro studies

ABSTRACT

Glioblastoma multiforme is one of the most aggressive cancer forms in humans, and has low recovery rates after surgery, ionizing radiation and chemotherapy. Therefore, there is a high interest in the development of new treatment methods, as for instance photodynamic therapy (PDT). It is here presented results of the cytotoxic properties of the novel compound N^1-(4-(4-(benzyl(methyl)amino)thieno[2,3-*d*]pyrimidin-6-yl)benzyl)-N^2,N^2-dimethylethane-1,2-diamine (**1**), which was found ten-fold more active on the rat glioma cell model F98 than the reference drug Temozolomide (TMZ). Further cell survival studies showed a profound increase in F98 cell death on UVA-radiation (330 nm, 0.5 mW/cm^2). Photochemical internalization induced delivery of compound **1**, but in contrast to the cytostatic drug Bleomycin, a higher cytotoxicity was not observed. Localization studies using fluorescence microscopy revealed that compound **1** readily internalized into the cytosol but did not enter the cell nucleus. The compound was shown to be a relatively weak epidermal growth factor receptor inhibitor, which is not likely to explain its cytotoxicity. However, the quantum efficiency for generation of singlet oxygen was 23%, suggesting generation of reactive oxygen species as one possible mechanism. Although more studies are needed to reveal detailed mode of action, compound **1** is a promising photosensitizer candidate for further development in tests of animal models.

1. Introduction

Glioblastoma multiforme (GBM) is a highly malignant brain tumor. Typical therapy includes surgery, radiotherapy, and chemotherapy. Temozolomide (TMZ) is one of the most used chemotherapeutic agents acting by methylation of guanine residues in DNA triggering cell death [1]. However, effective treatment of GBM is complicated by tumor heterogeneity, rapid proliferation, and infiltrating capacity as well as development of resistance towards drugs. Moreover, treatment with TMZ is linked to several adverse effects and there is a need to identify new efficient chemical agents with both a larger safety margin and a higher efficiency. Various kinase targets have been evaluated for therapy including epidermal growth factor receptor (EGFR) [2, 3], CDK4/6 [4], glycogen synthase kinase (GSK) [5], colony-stimulating factor 1 receptor (CSF-1R) [6], and kinases in the apoptotic pathway [7]. However, so far limited success has been obtained.

Thienopyrimidines are a class of heterocyclic compounds, which depending on their detailed substitution pattern possesses various biological activity [8–12]. Moreover, a number of thienopyrimidine derivatives have shown potent activity towards cancer cell lines and specific oncogenes [13–19].

Photodynamic therapy (PDT) is an established technique for clinical treatment of cancers. Briefly, a photosensitizer is administered to the tumor lesion, and by light activation, a photochemical reaction is initiated and eventually results in the generation of reactive oxygen species (ROS), which damage the membrane or internal cell functions to cause

* Corresponding author.
** Corresponding author.
E-mail addresses: odrun.gederaas@ntnu.no (O.A. Gederaas), bard.hoff@ntnu.no (B.H. Hoff).

https://doi.org/10.1016/j.jpap.2022.100114
Received 4 November 2021; Received in revised form 17 February 2022; Accepted 21 February 2022
Available online 1 March 2022

cell death [20, 21]. The molecular structure and chemical properties of a photosensitizer govern the wavelength of light needed, and the effective light dose and mechanisms of action by ROS production. Production of reactive free radicals is usually defined as a 'type I' reaction whereas processes that rely on singlet oxygen and related ROS are called 'type II' reactions. The localization of cellular damage (subsequent cellular or sub-cellular) depends on the hydrophobicity, charge, and chemistry of the designed molecules [22]. During the application of PDT on glioma or brain cancer, the drug or nanocarrier enters the systemic circulation and flows as per the blood distribution pattern [23]. In an overview of PDT molecules previously used for glioma treatment, Dubey et al. listed porphyrin-based PS, 5-aminolevulinic based molecules (5-ALA), and phthalocyanines [24].

The hydrophobic PDT molecules are often delivered by suitable carriers, liposomes [25], and dendrimers, while hydrophilic photosensitizers can be delivered in aqueous suspension for the treatment of gliomas. Other classes of drugs are explored for applications in PDT mediated glioma treatment, as the well-tested water-soluble 5-ALA, with a well known potential in PDT [26, 27].

Concerning delivery of the drug in the treatment of glioma, the blood-brain barrier (BBB) represents a very important obstacle and has been fundamental to blocking progress in development of new therapeutics for brain disorders as gliomas. Certain small molecule drugs may hovever cross the BBB via lipid-mediated free diffusion, providing the drug has a molecular weight <400 Da and forms <8 hydrogen bonds, while larger molecules can be reengineered with a Trojan horse delivery system to access receptor-mediated transport [28]. Madsen and Hirschberg concluded that crossing of BBB depends on light fluence and contrast by using focused ultrasound during their *in vivo* experiments on Fisher rats [29]. Their results showed that the technique causes sufficient opening of the BBB to allow the passage of a high molecular weight chemotherapeutic agent into glioma infiltrated brain. Photofrin associated PDT was used in the first randomized clinical trial on high-grade glioma [30], and followed up with 5-ALA based PDT in phase III randomized clinical trial [31], where 5-ALA is a precursor of the endogenous porphyrin photosensitizer, protoporphyrin IX. On the other hand, TMZ is the most common drug used to treat brain tumors such as glioblastoma multiforme or anaplastic astrocytoma [32]. However, PDT is a potential intervention for cancer treatment, and it is of major interest to identify new photosensitizers.

Herein, we have biologically evaluated compound **1**, (Fig. 1) by cell survival experiments in the rat glioma cell line F98, performed localization by fluorescence microscopy, and attempted photodynamic therapy on glioma cells. Compound **1** has a remarkably high cell activity compared to the established drug TMZ. The results of this study, using F98 glioma cells, are important for further *in vivo* PDT experiments. Thus, a rat glioma model (Fisher 344 rats) has recently been established at our lab where the same type of cells is instilled (orthotopic cancer model) and illuminated after drilling holes in the skull (unpublished). To document the fluorescing properties of compound **1**, both quantum yield and singlet oxygen were calculated and documented promising effects on cell death on rat F98 cells. Also, photodynamic therapy (PDT) by using UVA-radiation indicates intracellular accumulations in cytosolic compartments resulting in increased cellular death. The unique intervention process, photochemical internalization (PCI), involving the release of endocytosed macromolecules into the cytosolic matrix, is also evaluated for compound **1**. PCI was developed as a method for light-enhanced cytosolic release of membrane-impermeable molecules that have been taken up by cells and entrapped in endocytic vesicles [33].

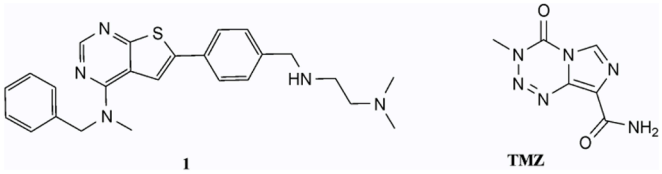

Fig. 1. Structure of N^1-(4-(4-(benzyl(methyl)amino)thieno[2,3-*d*]pyrimidin-6-yl)benzyl)-N^2,N^2-dimethylethane-1,2-diamine (**1**) and Temozolomide (TMZ).

2. Materials and methods

2.1. Chemicals

RPMI-1640 medium, L-glutamine, fetal bovine serum (FBS), sodium pyruvate, nonessential amino acids, trypsin, and phosphate-buffered saline (PBS) were obtained from Gibco BRL, Life Technologies (Inchinnan, Scotland). Gentamicin sulfate was purchased from Schering Corp (Kenilworth, NJ) and absolute ethanol from Arcus A/S (Oslo, Norway), the MTT solution; 3-(4, 5 dimethylthiazol-2-yl)−2, 5-diphenyl-tetrazoliumbromide) from Sigma-Aldrich (St. Louis, MO). Other chemicals were of the highest quality commercially available.

2.2. Synthesis of compound 1

2.2.1. N-Benzyl-6-bromo-N-methylthieno[2,3-d]pyrimidine-4-amine (3)

To 6-bromo-4-chlorothieno[2,3-*d*]pyrimidine (1.06 g, 4.22 mmol) was added *N*-benzylmethylamine (0.97 g, 8 mmol, 1.9 equiv.) and isopropanol (12 ml). The mixture was stirred under an N_2-atmosphere for 24 h at 80 °C until full conversion. After removal of the solvent, the product was diluted with diethyl ether (150 ml) and washed with water (3 × 50 ml). The combined organic phase was then washed with a saturated NaCl solution (20 ml), dried over anhydrous Na_2SO_4, filtered, and concentrated *in vacuo*. Purification using silica-gel column chromatography (EtOAc/*n*-pentane 1/5, $R_f = 0.30$) gave 1.16 g (3.48 mmol, 82%) of **3** as a pale yellow solid; mp. 129–130 °C, ^{1}H NMR (400 MHz, DMSO-d_6) δ: 8.35 (s, 1H), 7.71 (s, 1H), 7.38 - 7.31 (m, 2H), 7.30–7.24 (m, 3H), 5.03 (s, 2H), 3.35 (s, 3H); ^{13}C NMR (150 MHz, DMSO-d_6/$CDCl_3$): 169.4, 156.4, 152.5, 136.9, 128.3 (2C), 126.9, 126.7 (2C), 124.5, 115.6, 108.6, 53.6, 38.2; IR (neat, cm^{-1}): 1546, 1500, 1403, 1019, 969, 731, 697, 465. HRMS (TOF, ASAP+, *m/z*): found 334.0019, calcd for $C_{14}H_{13}N_3S^{79}Br$, $(M + H)^+$, 334.0014.

2.2.2. 4-(4-(Benzyl(methyl)amino)thieno[2,3-d]pyrimidin-6-yl) benzaldehyde (4)

N-Benzyl-6-bromo-*N*-methylthieno[2,3-*d*]pyrimidin-4-amine (800 mg, 2.39 mmol), 4-formylphenylboronic acid (431 mg, 2.87 mmol, 1.2 equiv.), Pd(PPh3)4 (128 mg, 111 μmol, 0.02 equiv) and K_2CO_3 (1.20 g, 8.68 mmol, 3.6 equiv.) were dissolved in a 1/1 solvent mixture of H_2O (8 ml) and 1,4-dioxane (8 ml). The mixture was stirred under an N_2-atmosphere for 2 h at 110 °C. The solvents were then removed, and the product was dissolved in EtOAc (100 ml) and washed with water (3 × 80 ml). The combined organic phases were then washed with a saturated NaCl solution (60 ml), dried over anhydrous Na_2SO_4, filtered, and concentrated *in vacuo*. Purification using silica-gel column chromatography (EtOAc/*n*-pentane, 1/3, $R_f = 0.27$) gave 356 mg (990 μmol, 41%) of **4** as a fluorescent yellow powder; mp. 139–142 °C; ^{1}H NMR (400 MHz, $CDCl_3$) δ: 10.00 (s, 1H), 8.50 (s, 1H), 7.91 – 7.84 (m, 2H), 7.68 – 7.54 (m, 2H), 7.62 (s, 1H), 7.44 – 7.28 (m, 5H), 5.08 (s, 2H), 3.44 (s, 3H); ^{13}C NMR (101 MHz, $CDCl_3$) δ: 191.3, 169.6, 158.5, 153.5, 139.4, 137.0, 136.4, 135.7, 130.4 (2C), 129.0 (2C), 127.7, 126.9 (2C), 126.3 (2C), 119.0, 116.9, 54.9, 38.6; IR (neat, cm-1): 1701, 1543, 1499, 1398, 1019, 966, 835, 812, 771, 725; HRMS (TOF, ASAP+, *m/z*): found 360.1175, calcd for $C_{21}H_{18}NOS$, $(M + H)^+$, 360.1171.

2.2.3. N^1-(4-(4-(Benzyl(methyl)amino)thieno[2,3-d]pyrimidin-6-yl) benzyl)-N^2,N^2-dimethylethane-1,2-diamine (1)

4-(4-(Benzyl(methyl)amino)thieno[2,3-*d*]pyrimidin-6-yl)benzaldehyde (106 mg, 294 μmol) and N^1,N^1-dimethylethane-1,2-diamine (30 mg, 340 μmol, 1.1 equiv.) were dissolved in dichloromethane (5 ml). The mixture was stirred for 4 h at room temperature. The solvent was then removed, before adding MeOH (10 ml) and $NaBH_4$ (20 mg, 582

μmol, 1.8 equiv.). The mixture was stirred for additional 4 h at room temperature. Water (30 ml) was added, and the mixture extracted with EtOAc (3 × 100 ml). The combined organic phases were washed with a saturated NaCl solution (30 ml), dried over anhydrous Na_2SO_4, filtered and concentrated *in vacuo*. Purification using silica-gel column chromatography (CH_2Cl_2/EtOH/NH_3, 70/30/2, $R_f = 0.20$) gave 87 mg (201 μmol, 68%) of **1** as a semi-solid; ^{1}H NMR (400 MHz, $CDCl_3$) δ 8.47 (s, 1H), 7.53 – 7.42 (m, 3H), 7.42 – 7.24 (m, 7H), 5.05 (s, 2H), 3.83 (s, 2H), 3.40 (s, 3H), 2.89 (br s, 1H), 2.73 (t, $J = 6.0$, 2H), 2.50 (t, $J = 6.0$ Hz, 2H), 2.25 (s, 6H); ^{13}C NMR (150 MHz, $CDCl_3$) δ 168.9, 158.3, 153.0, 140.4, 138.2, 137.3, 132.5, 128.9 (4C), 127.6, 127.0 (2C), 126.2 (2C), 117.1, 116.4, 58.8, 54.9, 53.5, 46.3, 45.4 (2C), 38.4; IR (neat, cm-1): 2965, 2817, 2770, 1550, 1534, 1320, 1016, 772, 731, 698; HRMS (TOF, ES+, *m/z*): found 432.2224, calcd for $C_{25}H_{30}N_5S$, $(M + H)^+$, 432.2222.

2.3. Cell culture

The cancer cell line F98 (ATCC No. CRL-2397™) is an undifferentiated malignant glioma cell line, originated from a fetal Fisher rat brain. The cells grown in monolayer and were contained in sterile cell culture flasks (75 cm^2, Corning). Incubation took place at 37 °C in a humidified atmosphere composed of air (95%) and CO_2 (5%). Dulbecco's modified Eagles medium (DMEM) with glucose (4.5 g/L) (Cat. No. BE12–604F, Lonza) supplemented with extra L-glutamine (80 mg/L), fetal bovine serum (FBS, 10%) and penicillin/streptomycin (100 U/mL).

2.4. Viability assay (MTT) post UVA – PDT/PCI treatment

The F98 cells were seeded in culture dishes (Corning/Sarstedt, (60 mm x 15 mm), at a density of 0.40 × 10^6 cells per dish (one day before PDT experiment) using a regular cultivation medium. A stock solution of compound **1** (10 mM, −20 °C, in DMSO, MW 431.6 Da, (Fig. 1) was thawed at room temperature and frozen immediately after preparing different concentrations (0–100 μM) in the first series of experiments. Total time of stock solution at 20 °C was about 30 min. Later, a fixed concentration (5 μM) was used in the PDT studies. After washing the cell dishes (PBS), the ordinary medium containing compound **1** (0–100 μM, 24 h, 37 °C, 5% CO_2) was added in the dark, and the cells were washed again (PBS) before exposing to UVA-radiation (330 nm, 0.5 mW/cm^2) in PBS using a Fluorolog 3 spectrophotometer before incubation overnight (37 °C, 5% CO_2). Cells containing only compound **1** were considered for "dark toxicity" assessments and samples without any treatment (nor light or photosensitizer) were used as controls. After the post-incubation period (24 h, 37 °C, 5% CO_2) the MTT proliferation assay was performed as shortly described [34]. The culture medium was removed, and cells were incubated in MTT-solution (0.5 mg/ml, 1 h, 37 °C, 5% CO_2) before replacing it with isopropanol (2 ml) and shaken on a plate shaker (30 min, 80 rpm). The important and modified step, as earlier described [35], included removing dead cells by centrifuging (5 min, 1500 rpm). The absorbance (595 nm) was measured using a Shimadzu UV-1700 spectrophotometer and the obtained data were processed and compared to untreated cells.

For the PCI experiments, the cells were seeded out in parallel with the PDT experiments using same cell number and were analysed with MTT assay at the same time. The PCI- treated dishes were incubated with a recommended concentration of the cytostatic drug BLM, using 0.1 μM (4 h, 37 °C), and treated with UVA-radiation (1 min) as explained in Section 2.5 at the end of BLM incubation period [34].

The photostability of compound **1** (5 μM in PBS) was characterized (absorption and fluorescence) using the same UVA-radiation periods (1–30 min) as described above in the PDT experiment on F98 cells (results section, Fig. 4). Also, one dish (5 μM in PBS) was incubated 24 h (37 °C, 5% CO_2) post 1 min of UVA-radiation to register a possible thermal change of the compound.

2.5. Light source

The light source for PDT treatment was composed of a 500 W Xenon Lamp taken from a spectrophotometer (Fluorolog 3, Horiba group, Japan), a broadband interference filter with maximum transmission at 330 nm (UVSIF 350 - 5523–2), and a plane aluminum mirror. The interference filter was selected to match the absorption spectrum of the sensitizer (Fig. 3). The integrated intensity at the cell level was 0.5 mW/cm^2 measured using a Coherent Fieldmaster (Vis Ca Srr. 202,060). After treatment by compound **1** (5 μM, 24 h) as described above, the culture dishes were UVA-radiated in the dark as illustrated in Figure S1 (left panel). The spectrum of the illumination source at the place of the sample was measured using an Ocean Optics Jaz spectrometer and is shown in Figure S1 (right panel).

2.6. Optical spectroscopy

UV–visible spectra were recorded on a Shimadzu UV-1601 PC spectrophotometer in dual-mode using 10-mm quartz cells. Steady-state photoluminescence measurements were carried out using a PTI Quantamaster 8075–22 (Horiba Scientific) equipped with Double Mono 300 spectrometer chambers for both excitation and emission. As a light source, the OB-75X (75 W Xenon arc lamp) was used. A Hamamatsu R928 PMT was used for detection in the range of 185 – 950 nm. For singlet oxygen luminescence detection, a port of the spectrometer using the 1427C-AH detector coupler together with liquid nitrogen cooled Indium-Gallium-Arsenide solid-state detector (Horiba Scientific: DSS-IGA020) was used. Data acquisition and basic data-handling were carried out with the Felix Data Analysis software. Post-processing and plot artworks were carried out using Matlab and Origin software, respectively.

The fluorescence quantum efficiency (QE) was determined using methanol as a solution with an optical density lower than 0.1 to avoid inner filter effects. By comparing the slope of the plotted fluorescence intensity *vs.* absorbance at a fixed excitation wavelength (340 nm) the QE is readily obtained using Coumarin 102 as reference (QE = 0.77 ± 0.06: This value was obtained by calibrating to the value obtained by Rurak and Spieles [36] using ethanol as solvent, QE: 0.764 ± 0.041).

Singlet oxygen yield was obtained by comparison with phenalenone (Sigma-Aldrich) as a reference, well known to have close to unity singlet oxygen quantum efficiency in many common solvents [37]. As the singlet oxygen generally shows a very weak signal in water and protic solvents, chloroform was chosen, as it is well known that halocarbons and non-aqueous solvents have generally higher ability to dissolve oxygen than protic solvents in the ambient atmosphere [38]. Moreover, the quenching mechanisms are here much slower (a few microseconds in water and 50 – 100 μs in organic solvents) giving rise to long lifetimes and consequently a stronger signal easier to detect with higher sensitivity and accuracy [39]. In these experiments, an 800 nm long-pass filter was used to block any visible light that might cause any higher order scattering through the spectrometer.

Time-resolved fluorescence decays were recorded using an IBH time-correlated single-photon counting (TCSPC) spectrometer system with a 1 nm resolved emission monochromator (5000 M, Glasgow, UK). The system was equipped with a TBX-04D picosecond photon detection module and the sample was excited using an IBH LED operating at 278 nm. The measured decay-trace was analyzed using deconvolution fitting with the IBH Data Station v 2.1 software. Additional details on the photophysical characterization procedures can be found by Lind et al [37]..

2.7. Fluorescence microscopy imaging

On day 1, cover slides (10 × 10 mm, $n = 3$) were placed onto the bottom of cell culture dishes before carefully adding F98 cell suspension (0.1 × 106 cells per dish, 3 mL) onto the top of the cover slides. The

dishes were further incubated for 24 h (37 °C, 5% CO_2). On Day 2, the old medium was removed, and the cover slides were washed with (PBS, 3 mL) before adding compound **1** solution in growth medium (5 μM, 3 mL) and further incubated (24 h, 37 °C, 5% CO_2). On day 3, the fluorescence microscopy imaging was performed at Altin BioTrix/Department of Biology, NTNU, Brattøra, Trondheim. The cover slides were removed from the culture dishes and placed on an object glass ensuring that the cells were on the side facing upwards before securing with a quartz coverslip. Fluorescence images were taken using a wide-field compound microscope (Eclipse 90i, Nikon Corp., Japan) by exciting the sample with a mercury lamp (HBO 103 W/2, Osram, Germany) fitted in a lamp holder (HMX-4B, Nikon Corp., Japan) equipped with a quartz collimator. Fluorescence was induced by applying a filter cube in the light path with a wide band exciter with a center wavelength of 330 nm (330WB80 filter, Omega optical, US) while monitoring emission at 435–485 nm (D460/50 M filter, Chroma Tech., US). To avoid crosstalk the excitation and emission were separated by a dichroic mirror in the cube with a cut-off at 400 nm. The images were captured with a CCD camera (DS-Fi1/DS-U2, Nikon Corp, Japan) on a computer running NIS-F (Nikon Imaging Software F, v.4.30.01, Nikon Corp., Japan). For optimal excitation in the UVA, a fluorite-objective with a high numerical aperture were used (40x S Fluor, NA 0.9, Nikon Corp., Japan) and quartz coverslips (Alfa Aesar, Germany). Corresponding images with differential interference contrasting were taken for navigational purposes in the fluorescence images.

3. Results

3.1. Synthesis of compound 1

N^1-(4-(4-(Benzyl(methyl)amino)thieno[2,3-*d*]pyrimidin-6-yl) benzyl)-N^2,N^2-dimethylethane-1,2-diamine (**1**) was synthesized through a four-step route, where the experimental set-up for the two first transformations was adopted from Bugge et al [15], see Scheme 1.

The preparation commences with a nucleophilic aromatic substitution on 6-bromo-4-chlorothieno[2,3-*d*]pyrimidine (**2**), with *N*-benyl-methylamine, proceeding regioselectively at C-4 in refluxing 2-propanol. Purification by silica-gel column chromatography gave 82% of intermediate **3**. To introduce the 6-aryl group, a palladium tetrakis catalyzed Suzuki cross-coupling between compound **3** and 4-formylphenylboronic acid was employed, giving the aldehyde **4** in 41% yield after silica-gel column chromatography. Lastly, the aldehyde function was converted to an amine by a one-pot two-step reductive amination. via the corresponding imine. Compound **1** was isolated in 68% yield after silica-gel column chromatography.

3.2. Cytotoxicity of compound 1 on F98 cells

To investigate cytotoxic properties of compound **1**, the F98 cell viability studies were initially carried out by incubation of **1** at different concentrations (0.1–100 μM) for 24 h, at 37 °C in the dark (Fig. 2) using TMZ as a positive control. The results indicate a 50% cell death (LD_{50}) of 20 μM and 200 μM for compound **1** and TMZ, respectively. Complete cell death was observed at 40 μM for **1** and at 1000 μM for TMZ. On basis of the above cytotoxicity measurements, it was chosen to examine compound **1** in light-induced PDT experiments.

Thus, the photosensitizing effects of compound **1** were examined on F98 cells post-incubation of the compound **1** (5 μM, 24 h, 37 °C) and exposed to 330 nm UVA-radiated (0.5 mW/cm^2) for 0–30 min. This wavelength was chosen as it matched the absorption maximum (Fig. 3), and resulted the viability as presented in Fig. 4. The cell viability being defined as a percentage of untreated F98 cells, showed a ~100% increase in cell death post 30 min of UVA-exposure. Of particular interest is the immediate decrease at 3 min and the further increase in cell survival to a plateau post 10 min of light treatment.

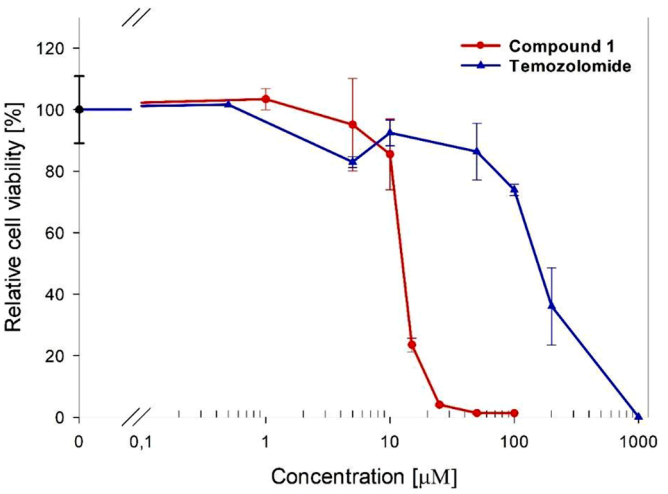

Fig. 2. Cytotoxic effects of various concentrations (0–1000 μM) of compound **1** compared to TMZ on F98 glioma cells as described in the materials and methods. Viability results from cells subjected to the same experimental protocol without chemicals and light. Each data point in the plots represents metabolic activity measured by MTT assay relative to cells incubated in a pyrimidine-free medium. The results are presented as mean values ± SD from five-seven separate experiments, all in duplicates.

3.3. Photophysical properties of compound 1

Compound **1** was assessed for basic photophysical properties relevant to PDT and fluorescence imaging. These experiments included the measurement of absorption and emission properties, along with the formation of singlet oxygen emission at 1275 nm due to energy transfer from the photosensitizer to molecular oxygen in the solvent.

The absorption and emission spectra of compound **1** (20 μM in methanol) are shown in Fig. 3 and illustrate an excitation maximum at ~ 330 nm and a fluorescence emission maximum at ~ 400 nm. The quantum efficiency (QE) was determined using Coumarin 102 as a reference with the same solvent (MeOH) and a value of 0.18±0.04 was obtained, see Fig. 5A. To elucidate the nature of the luminescence the lifetime of the light-emitting at 390–400 nm was measured using the time-correlated single photon counting technique, giving a relatively fast decay with two time-constants 0.21 and 0.90 ns contributing with 43 and 57% of the total amplitude, respectively (Fig. 5B). The moderate fluorescence QE is of large benefit to enable detection and localization of **1** in cell culture experiments to be discussed more below. Other solvents, such as PBS (pH 7.4), methanol, ethanol, and THF gave very similar spectra and time-resolved emissions, see Figures S2 and S3 for a comparison with methanol.

The photostability of compound **1** (5 μM in PBS) was characterized (absorption and fluorescence) using the same UVA-radiation periods (1–30 min) as shown in Figure S7. An UVA-exposure period of 30 min lowers the concentration of compound **1** with approximately 15–20%, concomitant with an increase of photoproducts absorbing at 400–450 nm. One minute of UVA-radiation followed by 24 h of incubation reduced the compound **1** concentration an additional 15–20%.

3.4. Singlet oxygen yield

In order to examine if the PDT effect was a type I or type II mechanism, the ability of the photosensitizer to produce singlet oxygen was examined, using phenalenone as reference [40]. The absorbance of the photosensitizer and the reference was first set to be approximately equal by adjusting the concentrations, see Fig. 6A. The absorbance values were found to be equal at 342 nm (Fig. 6A) and this wavelength was chosen as excitation in the singlet oxygen luminescence measurement (Fig. 6B). Note also that the absorbance here is well below 0.15 to avoid inner

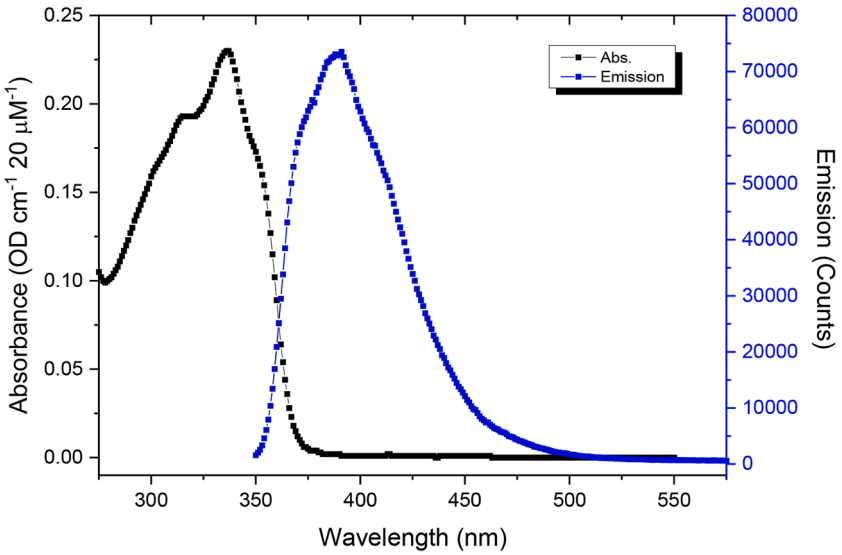

Fig. 3. Absorption and emission spectra of a diluted solution (20 µM) of compound **1** in methanol. The emission spectrum was obtained by excitation at 337 nm.

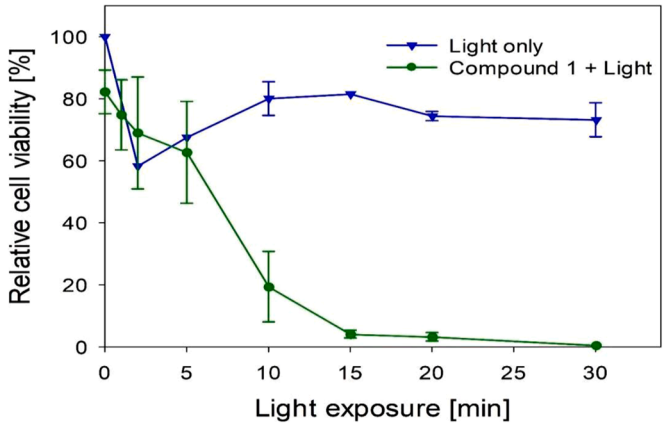

Fig. 4. Effects of photodynamic therapy (PDT) using compound **1** (5 µM, 24 h) on the survival of F98 rat glioma cells as a function of UVA-radiation (330 nm, 0.5 mW/cm^2), as described in "Material and Methods". The cell viability was measured by MTT assay 24 h post UVA-exposure. The results are presented as mean values ± SD from three separate experiments, all in duplicate cell dishes.

filter effects at the excitation wavelength. Integrating the singlet oxygen emissions as plotted in Fig. 6B, it can be concluded that the QE for **1** in $CHCl_3$ is approximately 20 - 23% relative to phenalenone [40]. Thus, the generation of singlet oxygen can explain the high activity of compound **1** in cell studies upon UVA exposure.

3.5. *Fluorescence microscopy of compound 1 incubated F98 cells*

To understand the compounds mode of action, we performed fluorescence microscopy and differential interference contrast (DIC) on F98 cells incubated with **1** (5 µM, 24 h, 37 °C, 5% CO_2). A representative selection of images is present in Fig. 7. In general, the images show outstretched F98 cells connected to each other, a typical form of brain cells. The F98 cells are quite sensitive to both washing and microscopy procedures, resulting in partly rolling-up cells (without dying) as present in the upper images of cells incubated with **1**, and analyzed by both fluorescence microscopy and differential interference contrast (DIC). The blue sections represent the fluorescence from **1** alone, indicating that the compound was internalized into the cells. It likely did not penetrate the nuclei, since no detectable fluorescence was observed there. The lower images show F98 control cells without treatment and no blue sections, meaning that there were no or negligible amounts of

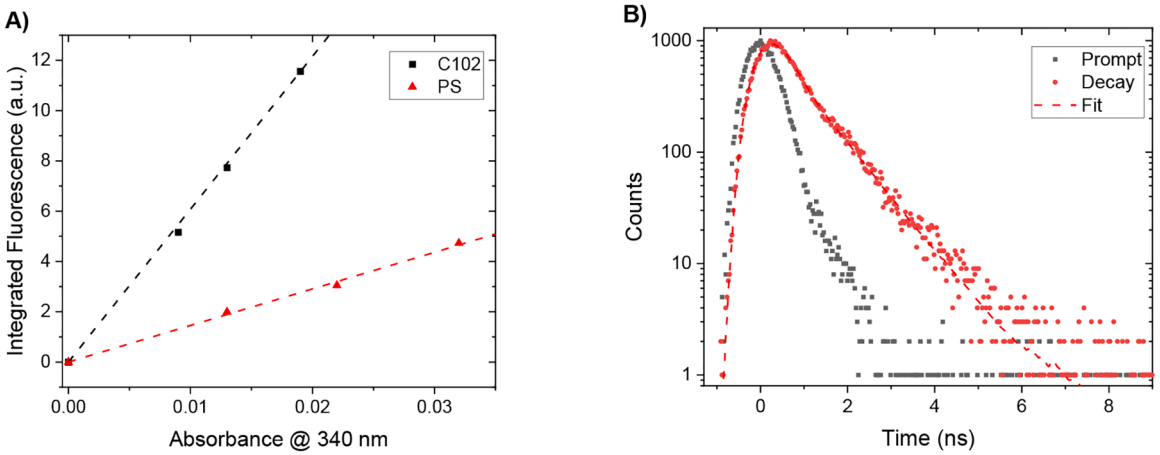

Fig. 5. A) Quantum yield measurements using Coumarin 102 as reference. The absorbance at 340 nm is here plotted *vs*. the total integrated emission. B) TC-SPC trace for excitation at 278 nm monitoring the emission at 400 nm. The black dots represent the system response (Prompt) whereas the dashed red curve is a deconvolution fit giving parameter as discussed in the text.

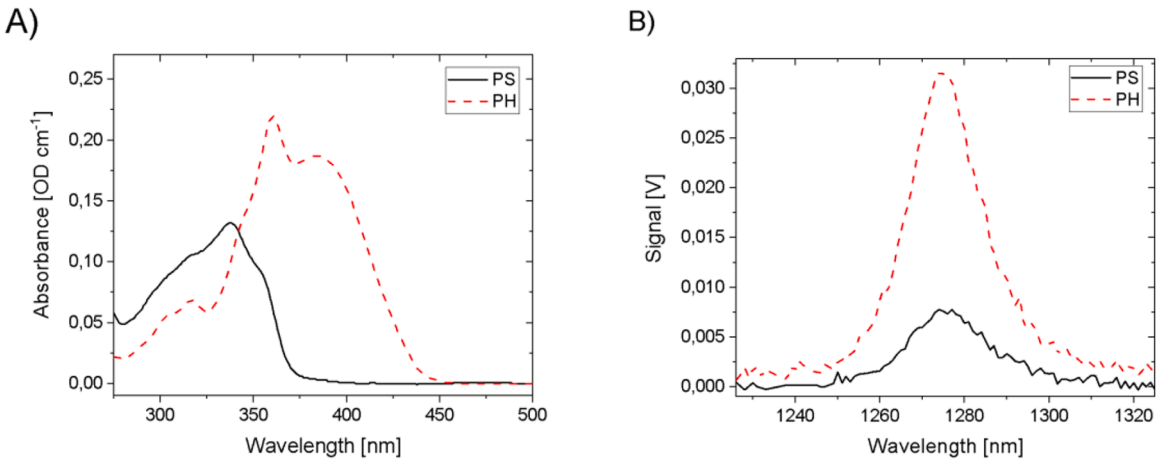

Fig. 6. A) Absorption spectra of compound **1** (PS) and the reference molecule phenalenone (PH) in $CHCl_3$. Note the absorbances coincide at 342 nm. B) The singlet oxygen spectrum centered at 1275 nm upon excitation at 342 nm. Slits were 16 and 8 nm for the excitation and emission spectrometers, respectively. Chloroform was used as a solvent.

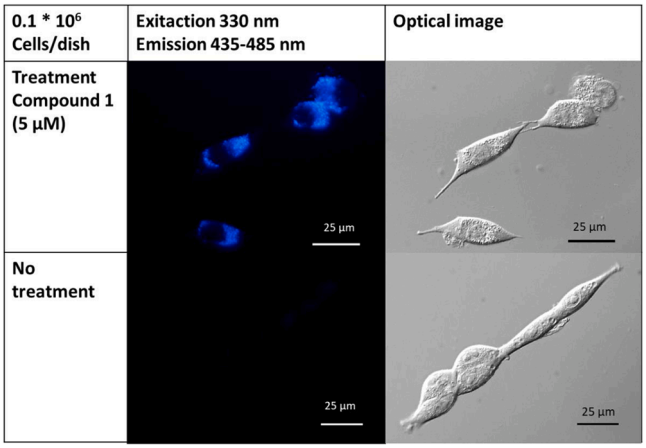

Fig. 7. Microscopy of identical F98 rat glioma cells by fluorescence microscopy (left images) and DIC (right images), taken 48 h post-treatment. Localization of blue fluorescence from compound **1** (5 µM, 24 h, 37 °C) is present in the upper left image, and no autofluorescence of untreated cells in the lower left image.

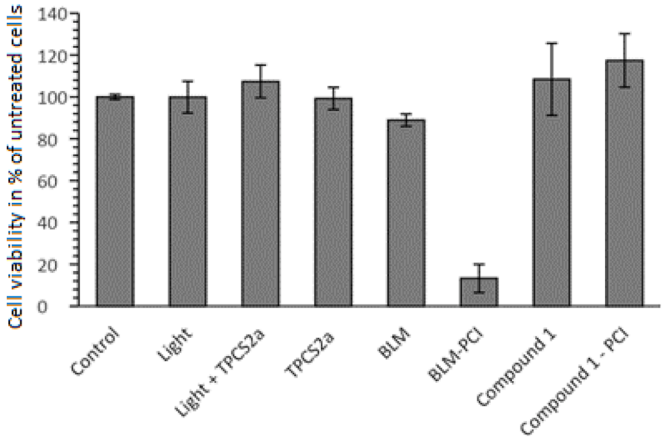

Fig. 8. Viability study of rat glioma cells (F98), post compound **1**-based PCI. The result presents% of treated cells relative to control cells. Bleomycin (BLM) was used as a "positive control" and the PCI treatment was performed by using the photosensitizer $TPCS_{2a}$ together with blue light as described in detail in material & methods. The PDT effects on F98 cells are not included but based on earlier information on F98 cells. Error bars are +/- SD from three parallels in three different experiments.

auto-fluorescence from the cells themselves at the wavelength used for excitation (330 nm) or the wavelengths monitored for emission (435–485 nm).

3.6. Photochemical internalization

The cytotoxicity effects by using photochemical internalization (PCI), was tested on F98 cells incubated with compound **1** and compared to the DNA alkylating anticancer drug bleomycin (BLM) (0.1 µM, 4 h, 37 °C) [35]. The results are present in Fig. 8 and indicate no increase in cytotoxicity after incubation of compound **1** (5 µM, 24 h, 37 °C, 5% CO_2) by the PCI technology using 1 min of UVA-exposure, compared to the effects of administrating only compound **1**. The largest reduction in cell viability was observed by the BLM-PCI (viability = 12.0% +/−3.5%) compared to BLM alone (viability = 90% +/−2.5%) indicating that BLM molecules were successfully internalized by this technology. The concentration 0.1 µM BLM was based on previous studies on both AY27 and F98 cells [35].

4. Discussion

This paper reports the four-step synthesis of a novel thienopyrimidine, compound **1** (Scheme 1), its photophysical properties, and its PDT effects on rat glioma cancer cells. Its absorption and emission properties are similar in both protic (PBS, methanol, ethanol) and aprotic ($CHCl_3$ and THF) solvents, with a moderate quantum efficiency (18%), making them useful for observation in cells using fluorescence microscopy. In general, cell survival is limited by high drug dosage and non-specificity [41]. Compound **1** is sufficiently soluble in a biocompatible formulation and able to pass cellular membranes where singlet oxygen has a longer lifetime [39] and induces stronger cytotoxic effects compared to aqueous environments, as described by Pushpan et al [42].. But fluorescence microscopy studies (Fig. 7) indicate that compound **1** also accumulates in the cytosolic compartments. The relative singlet oxygen yield of **1**, was determined by integrating the spectrum of the 1275 nm emission peak relative to that of phenalenone, giving a value of around 20% for the photosensitizer, and generation of ROS was enhanced with the increase of the PS concentration or the light dose, indicative of a type II PDT effect. The singlet oxygen yield is thus similar to the widely used $AlPcS_{2a}$ compound, although these studies used methanol or D_2O as solvent [43].

The immediate PDT effect on F98 cells with 3 min of light (Fig. 4) has

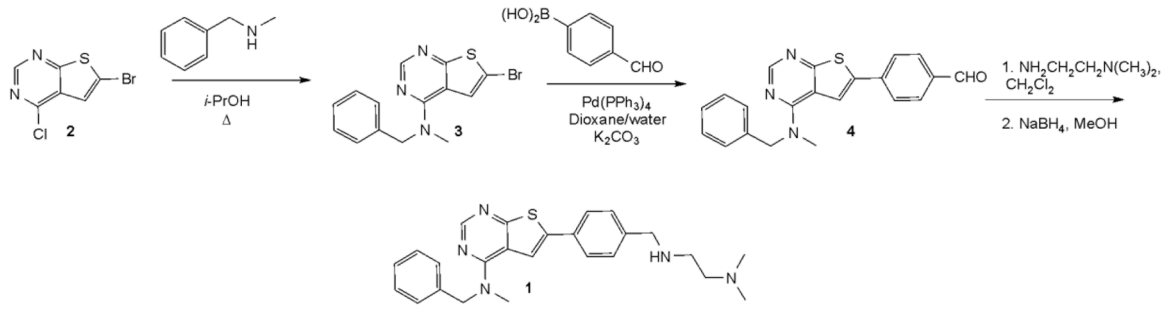

Scheme 1. Synthesis of N^1-(4-(4-(benzyl(methyl)amino)thieno[2,3-*d*]pyrimidin-6-yl)benzyl)-N^2,N^2-dimethylethane-1,2-diamine (**1**).

earlier been observed in both bladder cancer cell line (AY27) after incubation by Ru-porphyrin [44] and in human colon cancer cells (WiDr) by using 5-aminolevulinic acid [45]. The effect can partly be explained by DNA repair mechanisms which work well at low light doses as demonstrated in F98 during the first 10 min of UVA-radiation (Fig. 4). In absence of light (0 min), compound **1** (5 μM) exhibits relatively low toxicity (18%); as much as 82% of the cells were found to be metabolically active post-incubation. In contrast, there is substantial phototoxicity leading to LD_{50} at 7 min of light and complete cell death after 30 min of light exposure. The photostability of compound **1** has been investigated during the same time as the PDT studies and indicate that 30 min of UVA-radiation lowers the concentration of compound **1** with approximately 15–20% concomitant with an increase of photoproducts absorbing at 400–450 nm (Figure S7). However, the amount of photoproducts is not as pronounced as in the case of long irradiation and it can be concluded that compound **1** is reasonably stable for the concentrations and UVA-exposure times used in the PDT measurements.

Also, a study by Amawi et al. on a series of 13 thienopyrimidine derivates indicates oxidative stress as a mechanism of action in the three cancer cell lines HCT116, OV2008, and A2780 [13]. Our PDT results confirm that compound **1** is a promising photosensitizer candidate and an ideal molecule for glioma *in vitro* experiments while *in vivo* studies are still lacking. However, the mechanisms of action of compound **1** is still unclear. The structure is fairly similar to previously described EGFR inhibitors by Bugge et al [15].. Therefore, in parallel studies its enzymatic EGFR inhibitory activity has been measured (Supplementary Material, Figure S6). This shows a mediocre IC_{50} value of 77 nM, while the drug Erlotinib has an IC_{50} of 0.4 nM. Therefore, it is unlikely that the proven effect on F98 cells is due to inhibition of EGFR.

Fluorescence microscopy imaging, indicated that compound **1** was accumulated in cytosol of F98 cells, but without any entrance into the nuclei (Fig. 7). Further, it was attempted to use the photochemical internalization technology to enhance the endolysosomal release of anticancer drugs [46] and uptake of compound **1** by site-specific delivery. The PCI technology is still under development for delivery of different macromolecules, and the desulphonated tetraphenyl chlorin ($TPCS_{2a}$) from PCI Biotech AS, Oslo, was evaluated in this study to induce PCI by using compound **1.** In our earlier investigations involving two different anticancer agent's BLM and TMZ [35], it was documented that TMZ molecules most likely do not associate with endolysosomal compartments, because of the high activity of the DNA repair protein AGT (or MGMT) which confers resistance of F98 cells towards alkylating agents like TMZ [47]. But BLM was ideal as a positive control in the cell survival studies on F98 cells, and resulting in cell survival of only 12.0% +/−3.5 post 24 h after BLM incubation (0.1 μM) which is consistent with $TPCS_{2a}$-based PCI on the same cell line from our initial studies [35]. Compound **1** and TMZ are both examples of molecules that are not internalized by PCI in the F98 cell line. It should be mentioned that for the efficient crossing of BBB the molecular weight of **1** (431.6 Da) is rather high. Furthermore, the long-term chemical stability and the metabolic stability of compound **1** have yet to be investigated. Moreover, the work is of interest because compound **1** opens up for a new class of photosensitizers, but it remains to perform PDT experiments on other cancer cells.

5. Conclusions

Altogether, the novel compound N^1-(4-(4-(benzyl(methyl)amino) thieno[2,3-*d*]pyrimidin-6-yl)benzyl)-N^2,N^2-dimethylethane-1,2-diamine (**1**) documented distinctive photodynamic anti-tumor effects and low dark-toxicity in combination with UVA exposure, which suggests it as a useful lead compound and an ideal novel photosensitizer for development of anticancer agents. Also, compound **1** has shown to be both photo and heat stable during the present PDT study. However, compound **1** is not effective in combination with PCI technology. More detailed studies on these compounds and related references must be performed in parallel with *in vivo* experiments by using our established rat glioma orthotopic model in combination with PDT.

Acknowledgments

This work was partly supported by the Department of Chemistry, Norwegian University of Science and Technology, NTNU, Trondheim, together with operating costs from the Cancer Research Foundation of St. Olav's University Hospital, Trondheim. The authors want to thank Kristin Grenstad, Department of Physics, NTNU, for assistance during the *in vitro* experiments. We are also grateful to PCI Biotech AS, Oslo, for providing the $TPCS_{2a}$ compound as a positive control according to the PCI experiments.

Supplementary materials

Supplementary material associated with this article can be found, in the online version, at doi:10.1016/j.jpap.2022.100114.

References

[1] D. Fontijn, A.D. Adema, K.K. Bhakat, H.M. Pinedo, G.J. Peters, E. Boven, O6-Methylguanine-DNA-methyltransferase promoter demethylation is involved in basic fibroblast growth factor–induced resistance against temozolomide in human melanoma cells, Mol. Cancer Ther. 6 (2007) 2807–2815.
[2] R.G. Verhaak, K.A. Hoadley, E. Purdom, V. Wang, Y. Qi, M.D. Wilkerson, C. R. Miller, L. Ding, T. Golub, J.P. Mesirov, Integrated genomic analysis identifies clinically relevant subtypes of glioblastoma characterized by abnormalities in PDGFRA, IDH1, EGFR, and NF1, Cancer Cell 17 (2010) 98–110.
[3] M. Westphal, C.L. Maire, K. Lamszus, EGFR as a target for glioblastoma treatment: an unfulfilled promise, CNS Drugs 31 (2017) 723–735.
[4] S. Goel, Q. Wang, A.C. Watt, S.M. Tolaney, D.A. Dillon, W. Li, S. Ramm, A. C. Palmer, H. Yuzugullu, V. Varadan, Overcoming therapeutic resistance in HER2-positive breast cancers with CDK4/6 inhibitors, Cancer Cell 29 (2016) 255–269.
[5] R. Atkins, S. Stylli, R. Luwor, A. Kaye, C. Hovens, Glycogen synthase kinase-3β (GSK-3β) and its dysregulation in glioblastoma multiforme, J. Clin. Neurosci. 20 (2013) 1185–1192.
[6] S.J. Coniglio, E. Eugenin, K. Dobrenis, E.R. Stanley, B.L. West, M.H. Symons, J. E. Segall, Microglial stimulation of glioblastoma invasion involves epidermal growth factor receptor (EGFR) and colony stimulating factor 1 receptor (CSF-1R) signaling, Mol. Med. 18 (2012) 519–527.

[7] S.A. Valdés-Rives, D. Casique-Aguirre, L. Germán-Castelán, M.A. Velasco-Velázquez, A. González-Arenas, Apoptotic signaling pathways in glioblastoma and therapeutic implications, Biomed. Res. Int. (2017) 2017.
[8] J.F. Bower, A.W. Faull, J. Winter, Thienopyrimidines and thiazolopyrimidines for use in medicine, 2007, US Patent and Trademark Office, US 2007/0244133 A1.
[9] B.C. Shook, D. Chakravarty, J.K. Barbay, A. Wang, K. Leonard, V. Alford, M. T. Powell, S. Rassnick, R.H. Scannevin, K. Carroll, N. Wallace, J. Crooke, M. Ault, L. Lampron, L. Westover, K. Rhodes, P.F. Jackson, Substituted thieno[2,3-*d*] pyrimidines as adenosine A2A receptor antagonists, Bioorg. Med. Chem. Let. 23 (2013) 2688–2691.
[10] M.-.Y. Jang, S. De Jonghe, K. Van Belle, T. Louat, M. Waer, P. Herdewijn, Synthesis, immunosuppressive activity and structure–activity relationship study of a new series of 4-N-piperazinyl-thieno [2, 3-d] pyrimidine analogues, Bioorg. Med. Chem. Lett. 20 (2010) 844–847.
[11] M. Berger, B. Albrecht, A. Berces, P. Ettmayer, W. Neruda, M. Woisetschläger, S (+)-4-(1-phenylethylamino) quinazolines as inhibitors of human immunoglobuline E synthesis: potency is dictated by stereochemistry and atomic point charges at N-1, J. Med. Chem. 44 (2001) 3031–3038.
[12] W. Yang, L. Li, X. Ji, X. Wu, M. Su, L. Sheng, Y. Zang, J. Li, H. Liu, Design, synthesis and biological evaluation of 4-anilinothieno [2, 3-d] pyrimidine-based hydroxamic acid derivatives as novel histone deacetylase inhibitors, Biorg. Med. Chem. 22 (2014) 6146–6155.
[13] H. Amawi, C. Karthikeyan, R. Pathak, N. Hussein, R. Christman, R. Robey, C. R. Ashby Jr, P. Trivedi, A. Malhotra, A.K. Tiwari, Thienopyrimidine derivatives exert their anticancer efficacy via apoptosis induction, oxidative stress and mitotic catastrophe, Eur. J. Med. Chem. 138 (2017) 1053–1065.
[14] T.R. Rheault, T.R. Caferro, S.H. Dickerson, K.H. Donaldson, M.D. Gaul, A.S. Goetz, R.J. Mullin, O.B. McDonald, K.G. Petrov, D.W. Rusnak, Thienopyrimidine-based dual EGFR/ErbB-2 inhibitors, Bioorg. Med. Chem. Lett. 19 (2009) 817–820.
[15] S. Bugge, S.J. Kaspersen, S. Larsen, U. Nonstad, G. Bjørkøy, E. Sundby, B.H. Hoff, Structure–activity study leading to identification of a highly active thienopyrimidine based EGFR inhibitor, Eur. J. Med. Chem. 75 (2014) 354–374.
[16] A. Zhao, X. Gao, Y. Wang, J. Ai, Y. Wang, Y. Chen, M. Geng, A. Zhang, Discovery of novel c-Met kinase inhibitors bearing a thieno [2, 3-d] pyrimidine or furo [2, 3-d] pyrimidine scaffold, Biorg. Med. Chem. 19 (2011) 3906–3918.
[17] Y. Lv, M. Li, T. Liu, L. Tong, T. Peng, L. Wei, J. Ding, H. Xie, W. Duan, Discovery of a new series of naphthamides as potent VEGFR-2 kinase inhibitors, ACS Med. Chem. Lett. 5 (2014) 592–597.
[18] F. Han, S. Lin, P. Liu, X. Liu, J. Tao, X. Deng, C. Yi, H. Xu, Discovery of a novel series of thienopyrimidine as highly potent and selective PI3K inhibitors, ACS Med. Chem. Lett. 6 (2015) 434–438.
[19] A. Gryshchenko, V. Bdzhola, A. Balanda, N. Briukhovetska, I. Kotey, A. Golub, T. Ruban, L. Lukash, S. Yarmoluk, Design, synthesis and biological evaluation of N-phenylthieno [2, 3-d] pyrimidin-4-amines as inhibitors of FGFR1, Biorg. Med. Chem. 23 (2015) 2287–2293.
[20] Á. Juarranz, P. Jaén, F. Sanz-Rodríguez, J. Cuevas, S. González, Photodynamic therapy of cancer. Basic principles and applications, Clin. Trans. Oncol. 10 (2008) 148–154.
[21] D. Van Straten, V. Mashayekhi, H.S. De Bruijn, S. Oliveira, D.J. Robinson, Oncologic photodynamic therapy: basic principles, current clinical status and future directions, Cancers (Basel) 9 (2017) 19.
[22] A.P. Castano, T.N. Demidova, M.R. Hamblin, Mechanisms in photodynamic therapy: part two—cellular signaling, cell metabolism and modes of cell death, Photodiagnosis Photodyn. Ther. 2 (2005) 1–23.
[23] D. Kessel, M.G.H. Vicente, J.J. Reiners Jr, Initiation of apoptosis and autophagy by photodynamic therapy, Lasers Surg. Med. 38 (2006) 482–488.
[24] S.K. Dubey, S.K. Pradyuth, R.N. Saha, G. Singhvi, A. Alexander, M. Agrawal, B.A. Shapiro, A. Puri, Application of photodynamic therapy drugs for management of glioma, in: PORPHYRIN SCIENCE BY WOMEN: In 3 Volumes, World Scientific, 2019, pp. 162–174.
[25] V. Kushwah, S.S. Katiyar, A.K. Agrawal, R.C. Gupta, S. Jain, Co-delivery of docetaxel and gemcitabine using PEGylated self-assembled stealth nanoparticles for improved breast cancer therapy, Nanomed. Nanotechnol. Biol. Med. 14 (2018) 1629–1641.
[26] J. Kennedy, R. Pottier, D. Pross, Photodynamic therapy with endogenous protoporphyrin: IX: basic principles and present clinical experience, J. Photochem. Photobiol. B: Biol. 6 (1990) 143–148.
[27] J. Takahashi, S. Nagasawa, M.J. Ikemoto, C. Sato, M. Sato, H. Iwahashi, Verification of 5-aminolevurinic radiodynamic therapy using a murine melanoma brain metastasis model, Int. J. Mol. Sci. 20 (2019) 5155.
[28] W.M. Pardridge, Drug transport across the blood–brain barrier, J. Cereb. Blood Flow Metab. 32 (2012) 1959–1972.
[29] S.J. Madsen, H. Hirschberg, Site-specific opening of the blood-brain barrier, J. Biophotonics 3 (2010) 356–367.
[30] P.J. Muller, B.C. Wilson, Photodynamic therapy of brain tumors—a work in progress, Lasers Surg.Med. 38 (2006) 384–389.
[31] K. Mahmoudi, K. Garvey, A. Bouras, G. Cramer, H. Stepp, J.J. Raj, D. Bozec, T. Busch, C. Hadjipanayis, 5-aminolevulinic acid photodynamic therapy for the treatment of high-grade gliomas, J. Neurooncol. 141 (2019) 595–607.
[32] X.-.H. Tian, X.-.N. Lin, F. Wei, W. Feng, Z.-.C. Huang, P. Wang, L. Ren, Y. Diao, Enhanced brain targeting of temozolomide in polysorbate-80 coated polybutylcyanoacrylate nanoparticles, Int. J. Nanomedicine 6 (2011) 445.
[33] K. Berg, P.K. Selbo, L. Prasmickaite, T.E. Tjelle, K. Sandvig, J. Moan, G. Gaudernack, Ø. Fodstad, S. Kjølsrud, H. Anholt, Photochemical internalization: a novel technology for delivery of macromolecules into cytosol, Cancer Res 59 (1999) 1180–1183.
[34] O.A. Gederaas, A. Johnsson, K. Berg, R. Manandhar, C. Shrestha, D. Skåre, I. K. Ekroll, A. Høgset, A. Hjelde, Photochemical internalization in bladder cancer - development of an orthotopic *in vivo* model, Photochem Photobiol Sci 16 (2017) 1664–1676.
[35] O.A. Gederaas, A. Hauge, P.G. Ellingsen, K. Berg, D. Altin, T. Bardal, A. Høgset, M. Lindgren, Photochemical internalization of bleomycin and temozolomide–in vitro studies on the glioma cell line F98, Photochem. Photobiol. Sci. 14 (2015) 1357–1366.
[36] K. Rurack, M. Spieles, Fluorescence quantum yields of a series of red and near-infrared dyes emitting at 600− 1000 nm, Anal. Chem. 83 (2011) 1232–1242.
[37] P. Lind, D. Boström, M. Carlsson, A. Eriksson, E. Glimsdal, M. Lindgren, B. Eliasson, Structural, photophysical, and nonlinear absorption properties of trans-di-arylalkynyl platinum (II) complexes with phenyl and thiophenyl groups, J. Phys. Chem. A 111 (2007) 1598–1609.
[38] T. Sato, Y. Hamada, M. Sumikawa, S. Araki, H. Yamamoto, Solubility of oxygen in organic solvents and calculation of the Hansen solubility parameters of oxygen, Ind. Eng. Chem. Res. 53 (2014) 19331–19337.
[39] M. Bregnhøj, M. Westberg, F. Jensen, P.R. Ogilby, Solvent-dependent singlet oxygen lifetimes: temperature effects implicate tunneling and charge-transfer interactions, Phys. Chem. Chem. Phys. 18 (2016) 22946–22961.
[40] R. Schmidt, C. Tanielian, R. Dunsbach, C. Wolff, Phenalenone, a universal reference compound for the determination of quantum yields of singlet oxygen O2 (1Δg) sensitization, J. Photochem. Photobiol., A 79 (1994) 11–17.
[41] Y. Zheng, Z. Li, H. Chen, Y. Gao, Nanoparticle-based drug delivery systems for controllable photodynamic cancer therapy, Eur. J. Pharm. Sci. 144 (2020), 105213.
[42] S. Pushpan, S. Venkatraman, V. Anand, J. Sankar, D. Parmeswaran, S. Ganesan, T. Chandrashekar, Porphyrins in photodynamic therapy-a search for ideal photosensitizers, Current Med. Chemistry-Anti-Cancer Agents 2 (2002) 187–207.
[43] S.M. Bishop, A. Beeby, H. Meunier, A.W. Parker, M.S.C. Foley, D. Phillips, The photophysics of disulfonated metallophthalocyanines upon complexation with fluoride, J. the Chemical Society - Faraday Transactions 92 (1996) 2689–2695.
[44] V. Bogoeva, M. Siksjø, K.G. Sæterbø, T.B. Melø, A. Bjørkøy, M. Lindgren, O. A. Gederaas, Ruthenium porphyrin-induced photodamage in bladder cancer cells, Photodiagnosis Photodyn. Ther. 14 (2016) 9–17.
[45] O.A. Gederaas, A. Holroyd, S.B. Brown, D. Vernon, J. Moan, K. Berg, 5-Aminolaevulinic acid methyl ester transport on amino acid carriers in a human colon adenocarcinoma cell line¶, Photochem. Photobiol. 73 (2001) 164–169.
[46] B. Zhitomirsky, Y.G. Assaraf, Lysosomal accumulation of anticancer drugs triggers lysosomal exocytosis, Oncotarget 8 (2017) 45117.
[47] L.D. Rhines, P. Sampath, M.E. Dolan, B.M. Tyler, H. Brem, J. Weingart, O6-benzylguanine potentiates the antitumor effect of locally delivered carmustine against an intracranial rat glioma, Cancer Res 60 (2000) 6307–6310.